Compensation of corneal horizontal/vertical astigmatism, lateral coma, and spherical aberration by internal optics of the eye

Jennifer E. Kelly Department of Neurobiology and Behavior, Cornell University, Ithaca, NY, USA

Toshifumi Mihashi Technical Research Institute, Topcon Corporation, Tokyo, Japan

Howard C. Howland Department of Neurobiology and Behavior, Cornell University, Ithaca, NY, USA

Both the anterior surface of the cornea and the internal optics (the posterior cornea, crystalline lens) contribute to the aberration of a wavefront passing through the eye. Artal, Guirao, Berrio, and Williams (2001) reported that the wavefront aberrations produced by the internal optics offset, or compensate for, the aberrations produced by the cornea to reduce ocular wavefront aberrations. We have investigated the wavefront aberrations of the cornea, internal optics, and complete eye on both the population and individual level to determine which aberrations are compensated and probable paths leading to that compensation. The corneal and ocular aberrations of 30 young subjects at relaxed accommodation were measured with the Topcon Wavefront Analyzer, which simultaneously measures refraction, corneal topography (videokeratoscope), and wavefront aberrations (Hartmann-Shack sensor). We found strong evidence for compensation of horizontal/vertical (H/V) astigmatism (Zernike term Z5) lateral coma (Z8) and spherical aberration (Z12). H/V astigmatism compensation is scaled for each individual, suggesting that it is actively determined by a fine-tuning process. Spherical aberration shows no individual compensation, suggesting that is a passive result of genetically determined physiology. Lateral coma shows individually scaled compensation, some of which may be attributable to eccentricity of the fovea.

Keywords: monochromatic aberrations, compensation, horizontal/vertical astigmatism, lateral coma, spherical aberration

Introduction

Monochromatic optical aberrations of the human eye limit the optical quality of the image incident on the retina, and, consequently, the spatial resolution capabilities of the visual system. A fundamental question to address is what are the relative contributions of each optical element of the eye to the wavefront aberration of the complete eye?

Previous investigations have revealed that there is a balance between corneal aberrations and the aberrations of the internal optics of the eye that results in smaller ocular aberrations. Studies of the crystalline lens have shown that it has spherical aberration opposite in sign to that of the cornea, resulting in low ocular spherical error of various amounts (El Hage & Berny, 1973; Glasser & Campbell, 1998; Smith, Cox, Calber, & Garner, 2001). Artal and Guirao (1998), using double-pass retinal images and a keratoscope to separately examine the corneal and ocular wavefronts, found the same result for spherical aberration. They also found a reduction in third-order coma from the cornea to complete eye, and suggested that the lens compensates for corneal aberrations beyond spherical aberration and the clinically well known compensation of astigmatism.

Recently, Artal, Guirao, Berrio, and Williams (2001) used a Hartmann-Shack wavefront sensor and videokeratographic data to determine aberrations of the anterior cornea, the complete eye, and the internal optics (including the posterior corneal surface, the humors, and the crystalline lens) of nine subjects. They verified experimentally that direct subtraction of corneal aberrations from ocular aberrations gives accurate, in vivo measurements of internal aberrations. They found that both the cornea and the internal optics have larger overall aberrations than the complete eye, indicating that the two balance each other to improve the optical quality of the retinal image. The pattern of compensation varied with the type of aberration. For example, spherical aberration compensation was systematically patterned (corneal always negative, internal always positive), whereas coma compensation seemed random. This raises the question of whether compensation arises from passive, genetically determined physiology, or through an active, developmental feedback process.

Findings from studies of changing aberration structure with age provide further evidence of compensation between the coupled optical elements of the eye. For example, Artal, Berrio, Guirao, and Piers (2002) found a threefold increase with age in the magnitude of the root mean squared (RMS)

doi:10.1167/4.4.2 Received June 16, 2003; published April 16, 2004 ISSN 1534-7362

wavefront aberration of high-order terms of the complete eye for subjects ranging in age from 20 to 70 years. In young subjects, the wavefront aberration of the cornea was larger than that of the complete eye, interpreted as compensation by internal optics, but the opposite was true in older subjects, indicating a decoupling of the two elements and loss of balance between them.

However, Salmon and Thibos (2002) suggest caution before concluding compensation. They point out that if the corneal and ocular aberrations are measured on different axes, an artifact that looks like compensation will appear in the data due to the misalignment. In their examination of three subjects, they found evidence of both partial compensation and partial augmentation between the cornea and internal optics. Previous results, which did not account for misalignment, may have been subject to this type of error (Salmon and Thibos 2002).

We have further investigated compensation of the 2nd through 4th order Zernike wavefront aberrations of the cornea by the internal optics in 30 young subjects. We have examined both sample population means and individual values, which provide clues as to whether compensation arises passively or through an active process, as indicated by compensation scaled to each individual eye.

Methods

Subjects

Thirty healthy, normal subjects (24 female, 7 male) were recruited from the Cornell student body. Subjects' mean age was 20.5 years ± 0.4 SE, within –2D to +1D (equivalent sphere) of emmetropia, and of mean cylindrical error -0.41D ± 0.1 SE. Subjects showed no obvious ocular pathologies, had not undergone any sort of refractive surgery, and did not wear contact lenses. The research followed the tenets of the Declaration of Helsinki (1964) and was approved by the Human Subjects Committee of Cornell University.

Measurements

All measurements were made using a Topcon KR9000PW Wavefront Analyzer, a schematic of which is shown in Figure 1. The KR9000PW simultaneously measures refraction, ocular wavefront aberrations using a Hartmann-Shack wavefront sensor, and corneal wavefront aberrations using a videokeratoscope. Both wavefront aberration coordinate systems are computationally translated to center on the line of sight before Zernike coefficients (up to 6th order) are fit to the wavefront and reported.

Measurements were carried out in an ambient illumination of 23 lux to ensure that pupils were naturally dilated. Coefficients obtained refer to a 6-mm pupil. Three measurements were taken and averaged per eye, and each subject was measured in either one or both eyes.

During measurements, the subject rests his head securely against a chin rest and forehead bar and views a small fixation target (FT) of 2 deg in visual angle. Beam splitter BS1 reflects visible light for the optics of fixation target. The experimenter aligns the apparatus to the eye laterally by centering the observed corneal reflex of a parallel light beam from lens L1, and longitudinally by matching the heights of the images of two parallel light beams and of the second Placido ring, all of which have the same object height (details of the light sources are not shown in the figure).

The visual target (FT) is fogged due to decreasing vergence as it is optically distanced from the subject (L6). Refraction is measured with the subject focused at his or her far point.

Hartmann-Shack sensor

The ocular wavefront sensor consists of a Hartmann-Shack lenslet array (HSLA) of 163 lenslets, each an eight-level binary optical element (BOE) (lenslet size: 0.6-mm square; focal length: 40 mm; diffraction efficiency: 90 %) (Jahns & Walker, 1990), and a charge coupled device (CCD1). A super luminescent diode of central wavelength 840 nm and half width at maximum of 20 nm (SLD; Anritsu Corp., Atsugi, Japan) is attached to a polarization preserved optical fiber of core diameter 5.5 microns (PPOF). The end of the fiber serves as the point light source (PLS). A rotating d-prism in the common path of ingoing, and outgoing light scans the light beam on the fundus. A beam splitter (BS2) reflects light onto the eye. The SLD and the rotating d-prism reduce speckle and average the orientation and spatial discrepancy of reflectance from the fundus. During refraction and aberration measurements, the PLS is made conjugate with the fundus by adjustments of the location of lens L3 and the Hartmann-Shack sensor. The rotating d-prism is optically conjugate with the entrance pupil of the eye, the front focus of lenses L1 and L2 combined is on

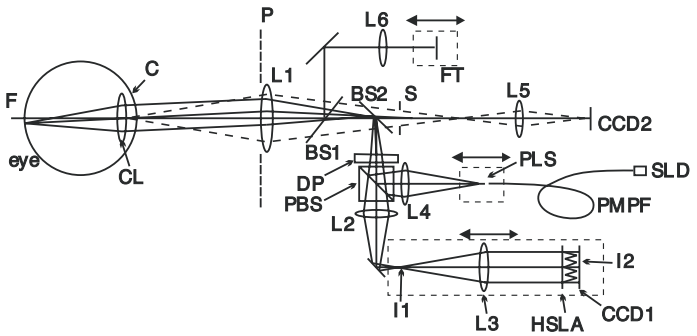

Figure 1. A schema of the KR9000PW Wavefront Analyzer (Topcon Corp., Tokyo, Japan). The components include a Hartmann-Shack lenslet array (HSLA), polarized beam splitter (PBS), point light source (PLS), polarization preserved optical fiber (PPOF), rotating d-prism (DP), additional lenses or groups of lenses (L1-6), and others that are explained in "Methods." The optical elements of the eye include the cornea (C) and the crystalline lens (CL).

the entrance pupil of the eye, and the back focus of lens L3 is on the Hartmann-Shack lenslet array. Thus while the d-prism is rotating and L3 and the H-S sensor are moving to adjust to the refraction of the eye, the conjugate relationship between the entrance pupil of the eye and the H-S lenslet array is always maintained, and the local information of the wavefront aberration from the Hartmann-Shack sensor always reflects the corresponding local wavefront information of the pupil of the eye.

To determine the ocular wavefront aberrations, the positions of the spots in the Hartmann-Shack image are used to calculate the slopes of rays from the lenslet array. The relation between the slopes and wavefront is

$$\frac{\partial W(X,Y)}{\partial X} = \frac{\Delta x}{f}, \qquad \frac{\partial W(X,Y)}{\partial Y} = \frac{\Delta y}{f}, \tag{1}$$

where $W(X, Y)$is the wavefront, X, Y, are horizontal and vertical coordinates on the pupil, Δx, Δy, are the displacements of the spots from their reference positions on the CCD, and f is the distance between the Hartmann-Shack lenslet array and the CCD (Thibos & Hong, 1999).

The accuracy of the Hartmann-Shack sensor was tested with repeated measures of a single surface model eye fabricated in the Topcon factory. Precision of measurements was computed as the mean of the SEs of measurements made for each subject and for the model eye.

Videokeratoscope

Corneal wavefront aberrations are measured using a videokeratoscope with 11 placido rings (P) of light source wavelength 950 nm. The image of the rings is observed by lens groups L1, L5, and a charge coupled device (CCD2), an optical arrangement that provides an image to the operator for the alignment of the machine to the subject's eye. A stop (S) inserted at the back focal point of lens L1 makes the optics telecentric, which means that the chief ray of a ray bundle from any position on the placido rings is parallel to the optical axis of the apparatus. The telecentric configuration can maintain a certain object/image magnification even if the objective distance changes. The corneal height map is computed from placido ring image heights by integrating from the corneal pole to periphery along 360 radians using a conic term and a 5th-order, one-dimensional polynomial. This height map is subtracted from a spherical surface with a radius computed from the placido ring image positions. The residual shape for the 7-mm diameter area centered on the corneal pole is then fit with Zernike polynomials up to the 6th order. The Zernike coefficients are multiplied by n-1, where n is the standard refractive index assigned to the cornea (1.3375), and added to the spherical aberration of the computed spherical surface to generate the aberrated wavefront. The wavefront coordinate plane is then translated so that the origin lies on the pupil center, and corneal wavefront aberration Zernike coefficients up to 6th order are calculated for a 6mm pupil.

The limitation on the accuracy of corneal wavefront aberration coefficients is the accuracy with which videokeratoscope height data is fit with Zernike polynomials to describe the corneal surface (Guirao & Artal, 2000; Howland, Glasser, & Applegate, 1992; Schwiegerling, Greivenkamp, & Miller, 1995). We confirmed that the Wavefront Analyzer's videokeratoscope both reasonably derives corneal shape from placido ring images and correctly computes corneal wavefront aberrations with respect to the line of sight. First we simulated the placido rings image that would be expected for a simple corneal shape, a sphere modulated by trefoil, following the method outlined by Rand, Howland, and Applegate (1997). From the simulated placido rings image, we calculated the Zernike coefficients to fit the 7-mm corneal surface using the Wavefront Analyzer program's algorithms. The calculated surface coefficients were checked against the actual coefficients of the assumed simple surface for accuracy.

We next checked that the WFA correctly shifted the axis along which corneal wavefront coefficients were calculated from the topographic axis (corneal pole) to the line of sight (pupil center). We modeled each eye's cornea with the optical design software program Code V (Optical Research Associates, version 9.30) using the 7-mm corneal Zernike surface description generated by the WFA videokeratoscope. The modeled corneal surface itself was shifted by the distance between the corneal pole and pupil center, and then corneal wavefront aberration coefficients were calculated for a 6-mm aperture. These Code V-generated corneal wavefront coefficients were checked against those reported by the WFA, which corrects for the shift after deriving the shape of the wavefront rather than by first translating the corneal surface. A single image of the spherical model eye was likewise analyzed to check the accuracy of the axis shift. Corneal wavefront coefficients were repeatedly computed as the origin of the calculations was progressively shifted away from the apex of the model eye using a modified version of the WFA program. These coefficients were checked against Code V's output for shifts of the same magnitude for a modeled surface with the specifications of the model eye.

Data analysis

All statistical tests were carried out in the software package Statview (SAS Institute, Inc., version 5.0.1.)

Only one eye per subject was included in each analysis to preserve the independence of the data. When both eyes had been measured, we arbitrarily chose to use the left eye on the assumption that the magnitude of aberrations of the left and right eyes correlate, as demonstrated by Smolek, Klyce, and Sarver (2002; also see below). The signs of bilaterally asymmetrical Zernike coefficients Z3, Z8, Z9, Z10, and Z11 were reversed for right eyes to account for the enantiomorphism of the right and left eyes (Howland &

Howland, 1977; Smolek et al., 2002). In all cases, we used normalized Zernike coefficients.

Wavefront aberrations due to internal optics were determined by simple subtraction of ocular from corneal Zernike coefficients (Artal et al., 2001) We tested the compensatory role of the internal optics by comparing the Zernike coefficients for 2nd through 4th order aberrations, first considering the sample population's mean absolute values using a Wilcoxon signed rank test and then considering individual subject values by examining correlations. High-order compensation was compared to ocular high-order RMS wavefront error, inclusive of all 3rd through 6th order coefficients. Statistical significance was set to the $p < .05$ level.

The lateral distance between the center of the pupil (origin of H-S sensor measurements) and the first Purkinje image (origin of unadjusted topographic measurements) at the entrance pupil as measured by the Wavefront Analyzer was compared to the magnitude of the lateral coma coefficient (Z8) using linear regression to examine the role of the eccentricity of the fovea and the pupil in producing coma (van Meeteren & Dunnewold, 1983). For comparison, an eccentric fovea and pupil were modeled in schematic eyes proposed by Navarro, Santamaria, and Bescos (1985) and by Liou and Brennan (1997) using Code V.

Results

Accuracy and repeatability

The ocular wavefront reported by the WFA for the model eye differed from what was expected (based on factory specifications) by a mean ± *SD* of only 0.030 ± 0.009 microns RMS wavefront error. The 4th-order spherical aberration coefficient had a SE of 0.0024 microns for 27 measurements. Measurements were also highly repeatable. For the 30 subjects used in this study, the mean RMS SE of the aberrated ocular wavefront was 0.0601 microns for astigmatism plus 3rd through 6th order coefficients, and 0.0467 microns for only 3rd through 6th order coefficients. Mean RMS SE of Zernike coefficients Z5, Z8, and Z12, those of interest to this study, were 0.0281 microns, 0.0139 microns, and 0.0107 microns, respectively.

When corneal surface fitting accuracy was tested with a simulated placido ring image that assumed a corneal shape with 3.54 microns of trefoil, the WFA algorithm calculated a trefoil of 3.41 microns and attributed a residual RMS of 0.16 microns to other terms, a reasonable match. Corneal wavefront coefficients generated by Code V from the shifted corneal surface differed from those calculated by the WFA by a mean RMS of 0.0523 ±.013 *SD* microns for astigmatism plus all 3rd through 6th order coefficients. Corneal wavefront aberrations generated by Code V for the shifted model eye differed from those calculated by the WFA program by a mean RMS of 0.0019 ± 0.0044 *SD* microns for all 3rd through 6th order coefficients.

Corneal wavefront coefficient repeatability was similar to that of ocular coefficients'. For the 30 subjects used in this study, the mean RMS SE of the aberrated corneal wavefront was 0.0933 microns for astigmatism plus 3rd through 6th order coefficients, and 0.0764 microns for only 3rd through 6th order coefficients. Mean RMS SE of Zernike coefficients Z5, Z8, and Z12, those of interest to this study, were 0.0415 microns, 0.0190 microns, and 0.0160 microns, respectively.

Bilateral symmetry

We checked our assumption of symmetry of aberrations between left and right eyes by comparing 2rd and 4th order coefficients (excluding defocus) for 13 subjects. We found highly significant Pearson correlations between right and left eye ocular coefficients ($r = 0.717$, Fisher's $p < .0001$) corneal coefficients ($r = 0.829$, Fisher's $p < .0001$) and internal coefficients ($r = 0.821$, Fisher's $p < .0001$). Figure 2 shows the dataset superimposed on the line $y = x$, which demonstrates perfect symmetry.

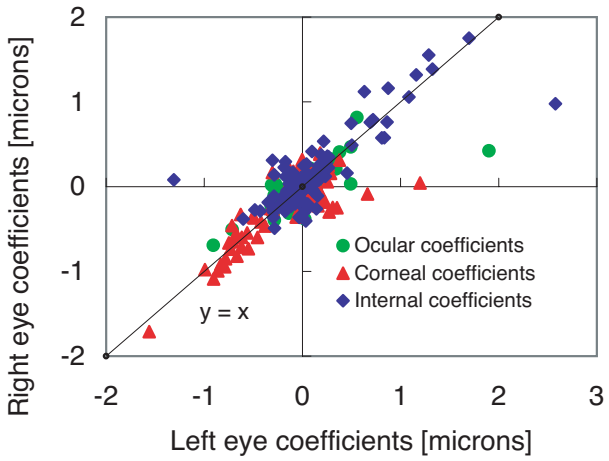

Figure 2. For each individual, the right and left eye ocular, corneal, and internal 2nd through 4th order Zernike coefficients (excluding defocus) are significantly correlated ($r = 0.717$, 0.829, 0.821, respectively; all $p < .001$). Here they are plotted against the line $y = x$, which is the plot of exact symmetry.

Sample-wide compensation

We investigated Zernike terms Z3 through Z14, with the exception of Z4, the term generated by defocus, for evidence of compensation between corneal wavefront aberrations and internal optics aberrations. For each term we compared the mean absolute value of the corneal aberration coefficient with the mean absolute value of the ocular aberration coefficient ($n = 30$, Figure 3). A decrease in magnitude between corneal and ocular coefficient means indicates compensation by internal optics to reduce overall aberrations, as corneal and internal coefficients add to give ocular coefficients. Because we are examining absolute values, overcompensation and undercompensation are indis-

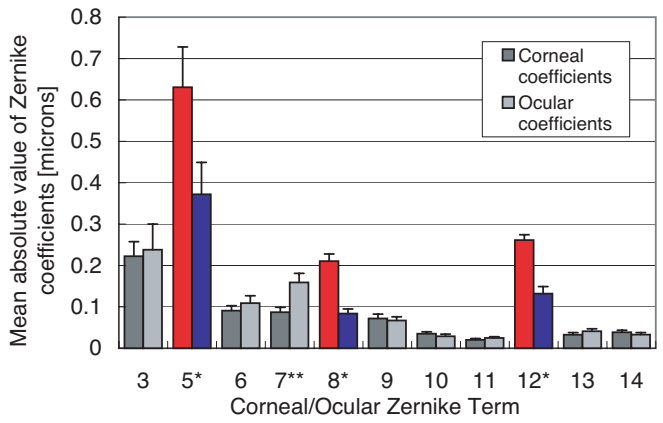

Figure 3. Of Zernike terms Z3 through Z14 (excluding defocus, Z4), the mean absolute values of the ocular coefficients of horizontal/vertical astigmatism (Z5), lateral coma (Z8), and spherical aberration (Z12) of 30 subjects were significantly reduced compared to corneal coefficients, indicating compensation by internal optics to reduce overall aberrations. Vertical coma (Z7) for the whole eye was significantly larger than for the cornea alone.

tinguishable. However, any reduction in corneal aberration will, in general, improve the optical quality of the eye.

Comparisons of the absolute values of corneal and ocular coefficients using a Wilcoxon signed rank test showed significant compensation for horizontal/vertical astigmatism (Z5, p = .0429), lateral coma (Z8, p = .009), and spherical aberration (Z12, p = .004). The mean coefficient values, listed in Table 1, show that H/V astigmatism was reduced by 41%, lateral coma reduced by 51%, and spherical aberration reduced by 36%. All other Zernike terms, including oblique astigmatism (Z3), did not show significant compensation. However, ocular vertical coma (Z7) was significantly larger than corneal vertical coma (p = .003).

The mean reduction in total high-order aberration RMS (3rd - 6th order RMS [microns]) that compensation introduced was 0.087 microns by lateral coma compensation and 0.075 microns by spherical aberration compensation, totaling 0.114 microns of compensation by the two combined. The mean total high-order RMS wavefront error values measured by the Wavefront Analyzer were 0.371 ± 0.015 SE microns for the cornea and 0.318 ± 0.023 SE microns for the total eye, a total high-order compensation of 0.053 microns. Therefore, roughly half of the reduction in RMS wavefront error introduced by compensation of lateral coma and spherical aberration was seen in the reduction of the total RMS wavefront error, which includes all 3rd through 6th order aberration coefficients.

Individual compensation

The previous results are indicative of general compensation in the entire sample group. We further investigated horizontal/vertical astigmatism (Z5), lateral coma (Z8), and spherical aberration (Z12) on an individual basis by testing for linear correlations between internal and corneal coefficient magnitudes. A significant correlation coefficient indicates that the magnitudes of an individual's internal and corneal coefficients are closely associated. Figure 4 shows a diagrammatic plot of internal coefficient magnitude against corneal coefficient magnitude. The location of an individual data point relative to the lines $y = -x$ and $y = -2x$ shows if that individual eye exhibits perfect compensation, overcompensation, undercompensation, or augmentation. We have included the reference line $y = -x$ on the scatter plots of Z5, Z8, and Z12 internal against corneal coefficients (Figures 5, 6, and 7).

We found a significant negative correlation (df = 29, r = -0.524, p = .0025) between internal and corneal horizontal/vertical astigmatism (Z5), as shown in Figure 5. The subject responsible for the obvious outlier has a cylinder of –2.3D, but a sphere of +1.0D, so her equivalent sphere, -0.167D, falls within our chosen range of acceptable deviation from emmetropia. Her large degree of astigmatism is seen in the horizontal/vertical Z5 astigmatism coefficient. When this outlier is excluded, the result is still significant (df = 28, r = –0.669, p < .001).

Aberration	RMS Mean ± SE [microns]		Reduction (corneal to ocular)		p value
	Corneal	Ocular	RMS [microns]	% C coef	
H/V Astigmatism (Z5)	0.634 ± 0.097	0.372 ± 0.077	0.262	41%	0.043
Lateral coma (Z8)	0.171 ± 0.016	0.084 ± 0.011	0.087	51%	0.009
Spherical aberration (Z12)	0.207 ± 0.012	0.132 ± 0.017	0.075	36%	0.004

Table 1. Mean absolute values of corneal and ocular Zernike coefficients showing significant compensation: h/v astigmatism, lateral coma, and spherical aberration. Of all 2nd through 4th order Zernike terms (excluding defocus), only these aberrations showed significant compensation of corneal aberrations by internal optics, as indicated by smaller ocular coefficients than corneal coefficients. Compensation is given in terms of RMS wavefront error reduction (microns) and in percentage reduction of each term's corneal coefficient value (% C coef). *P* values, indicating significant reductions, are for Wilcoxon signed rank tests, and were Bonferroni-corrected by multiplying each by the number of tests performed, 11, to control for repeated tests on the same dataset.

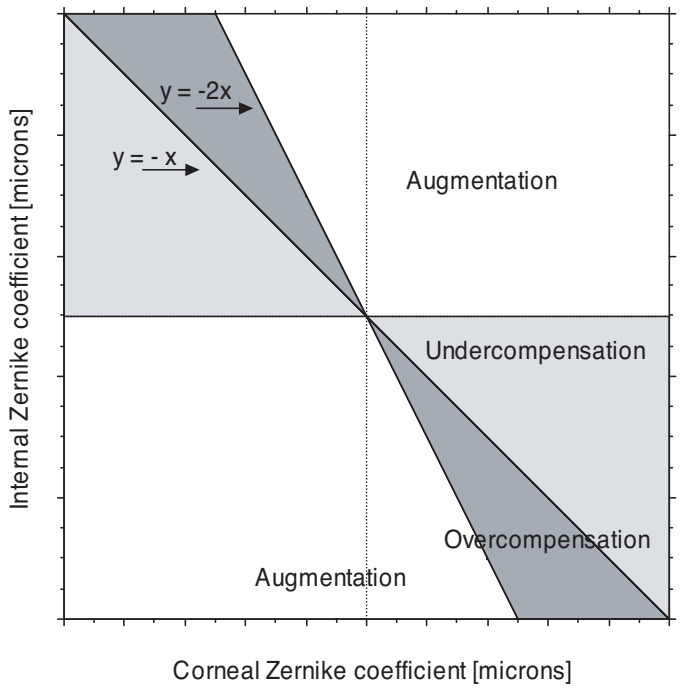

Figure 4. The relative values of corneal and internal Zernike coefficients determine if the magnitude of the ocular wavefront aberration will be larger or smaller than the corneal wavefront aberration. Perfect compensation (an ocular coefficient of zero) occurs when internal and corneal coefficients are of the same magnitude but opposite signs ($y = -x$). Undercompensation and overcompensation by the internal optics will both result in decreased magnitude of ocular coefficients. Augmentation occurs if both coefficients are of the same sign, or if they are of opposite signs and the internal coefficient is of greater magnitude than the corneal coefficient ($y = -2x$).

It is important to note that for our pool of 30 subjects, 17 had cylindrical refractive errors, 14 in the horizontal or vertical meridians, but only three in the oblique meridians. Inclusive of all subjects, individual dioptric refractive cylindrical error was significantly correlated with the absolute value of the ocular H/V astigmatism Zernike coefficient Z5 ($r = –0.886$, $p < .001$), but not with ocular oblique astigmatism, coefficient Z3. When the 3 subjects with oblique cylindrical refractive error are examined separately, 2 show both Z3 and Z5 compensation, and 1 shows both Z3 and Z5 augmentation. Three subjects is not a sufficient pool to draw conclusions concerning the ties between oblique refractive error meridians and possible oblique astigmatism Zernike wavefront compensation.

There was a significant negative correlation ($df = 29$, $r = -0.381$, $p = .0372$) between internal and corneal lateral coma (Z8), as shown in Figure 6.

Spherical aberration, Z12, does not show a similar pattern of individual compensation, as can be seen in Figure 7. The corneal coefficient is not significantly correlated with the internal coefficient ($df = 29$, $r = -0.289$, $p = .123$).

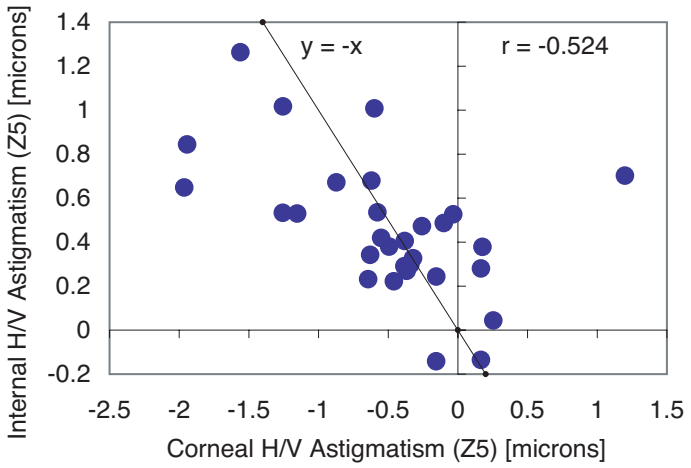

Figure 5. There is a significant negative correlation between internal and corneal horizontal/vertical astigmatism coefficients (Z5). The dotted line $y = -x$ shows the expectation of perfect compensation. The subject responsible for the outlier had a cylinder refraction of -2.3D but an equivalent sphere of 0.17D, within our range of acceptable ametropia.

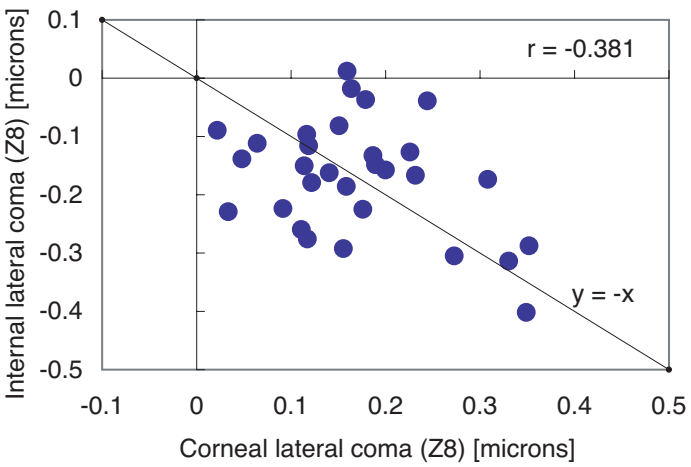

Figure 6. There is a significant negative correlation between internal and corneal lateral coma coefficients (Z8). The dotted line $y = -x$ shows the expectation of perfect compensation.

We further investigated lateral coma (Z8), spherical aberration (Z12), and total high-order compensation in relation to total ocular high-order RMS error. There is no correlation between the magnitude of total ocular high-order RMS and either ocular lateral coma or ocular spherical aberration. The magnitude of lateral coma plus spherical aberration compensation in RMS (microns) (Z8 + Z12, Figure 8a), or of either term alone (not shown), was not correlated to the magnitude of total ocular high-order wavefront error. However, the magnitude of total high-order compensation (the reduction in magnitude from corneal to ocular wavefronts observed inclusive of all 3rd through 6th order terms)

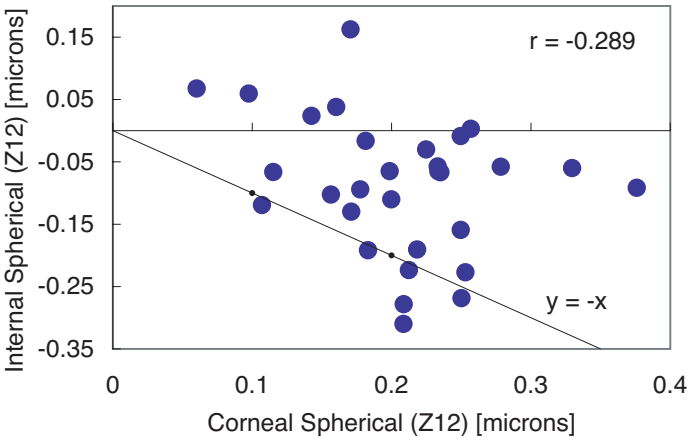

Figure 7. There is no significant correlation between internal and corneal spherical aberration coefficients (Z12). The dotted line *y* = -*x* show the expectation of perfect compensation.

was significantly negatively correlated with increasing total ocular wavefront error (r = -0.749, p < .0001, Figure 8b). There is no correlation between ocular total high-order RMS error and corneal total high-order RMS error (Figure 8c).

We next examined the relationship between lateral coma and the distance between the first Purkinje image and the pupil center. Both angle kappa, the angle between the line of sight (fovea to target) and the optic axis (center of the pupil to pole of the cornea), and eccentricity of the pupil, two causes of lateral coma, can cause noncoincidence of the first Purkinje image and the pupil center. As shown in Figure 9, ocular Zernike coefficients showed no relationship to the distance between the Purkinje image and pupil center. Corneal lateral coma coefficients increased significantly with increasing distance (regression coef = 0. 309, df = 29, F = 4.858, p = .036, r^2 = 0.148). Internal lateral coma coefficients decreased significantly with increasing distance (regression coef = -0.374, df = 29, F = 6.125, p = .0196, r^2 =.179).

A decentered or tilted lens with spherical aberration gives rise to lateral coma (van Meeteren & Dunnewold, 1983), so we investigated how the coefficients of spherical aberration (Z12) and the coefficients of lateral coma (Z8) correlate, but found no significant relationships.

To investigate the possible effects of angle kappa and pupil eccentricity on lateral coma, we ran ray-tracing simulations through two finite schematic eye models of Navarro et al. (1985) and Liou and Brennan (1997). Both have aspheric surfaces to reduce spherical aberration. The Navarro et al. schematic calls for a uniform refractive index lens and has spherical aberration that borders on the upper limits of measured human spherical aberration (Smith, 1995). The Liou and Brennan schematic incorporates a gradient index (GRIN) lens and has spherical aberration

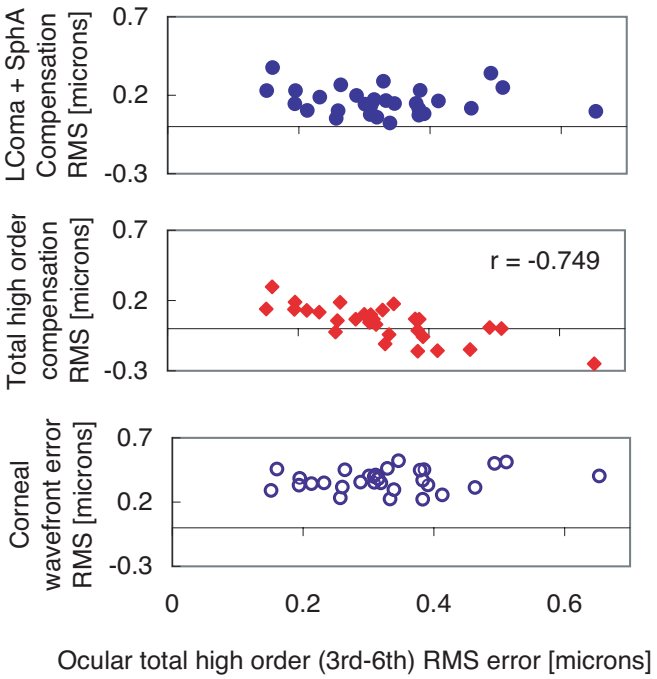

Figure 8. (a). The magnitude of lateral coma + spherical aberration (Z8+Z12) compensation is not correlated with increasing ocular high-order (3rd – 6th order) RMS wavefront error (microns). (b). Total high-order compensation is negatively correlated with increasing ocular wavefront error (r = -0.749, p < .0001). (c). Corneal high-order wavefront error is not correlated with increasing ocular wavefront error.

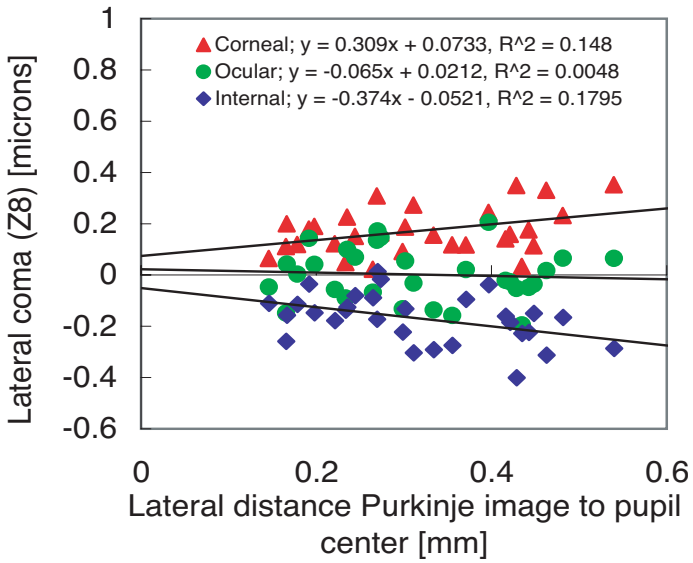

Figure 9. As lateral distance between the first Purkinje image and the pupil center increases, ocular (●) lateral coma coefficients (Z8) show no significant pattern of increase or decrease. Corneal (▲) coefficients increase significantly, while internal (◆) coefficients decrease significantly.

reported to match population mean values of humans as given in the literature (Liou & Brennan, 1997).

We show in Figure 10 that in both schematic eye models, internal compensation of lateral coma is generated automatically when wavefront measurements are taken at an off-axis field angle. The difference between the uniform index lens (a) and GRIN lens (b) is seen in the difference in the magnitude of compensation for the two models. Figure 11 demonstrates how horizontally shifting the pupil effects lateral coma measurements. Here the difference between the two schematic eyes is more apparent, as the uniform index model (a) has a larger amount of ocular aberration than corneal, whereas the GRIN model (b) generates automatic compensation with pupil shifting. Both models are limited approximations of real human eyes, but still demonstrate the possible compensatory outcomes of adjusting the placement and alignment of the eye's optical elements.

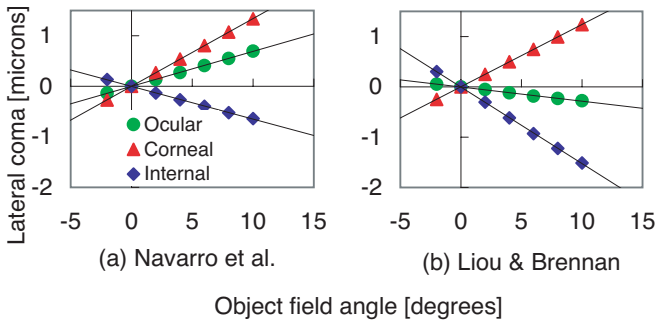

Figure 10. Ray-tracing (587.56 nm) through the Navarro et al. (1985) (a) and Liou and Brennan (1977) (b) schematic eyes shows that as the field angle of incoming rays increases, internal optics automatically compensate in proportion to corneal aberrations to reduce ocular lateral coma coefficients.

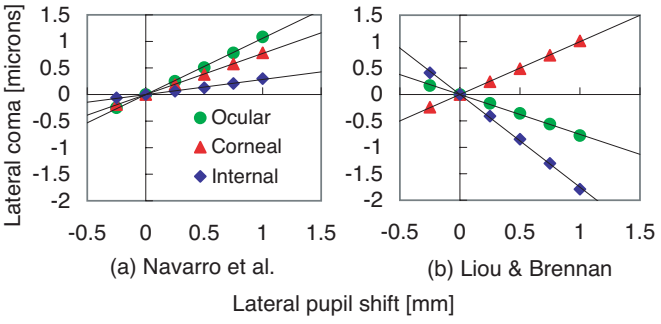

Figure 11. Ray-tracing (587.56 nm) through the Navarro et al. (1985) schematic eye (a) shows that as the pupil is decentered, internal optics coma adds upon corneal coma, resulting in greater levels of ocular coma. In contrast, shifting the pupil laterally in the Liou and Brennan (1977) schematic eye (b) automatically generates internal coma that compensates corneal coma, resulting in lower levels of ocular coma.

Discussion

Of all the aberrations contributing to the total wavefront aberration of the eye, the terms that showed significant compensation of corneal aberrations by internal optics at relaxed accommodation were horizontal/vertical astigmatism (Z5), lateral coma (Z8), and spherical aberration (Z12). The reduction of the mean magnitude of these aberrations in the complete eye is an important part of producing a retinal image of high optical quality. In the wavefront error due to high-order aberrations (3rd through 6th order), roughly half of the RMS reduction introduced by compensation of corneal lateral coma and corneal spherical aberration (0.114 microns) was still detected in the reduction in total RMS wavefront error (from 0.371 microns corneal RMS to 0.318 microns ocular RMS). That only half is seen is probably attributable to wavefront error introduced by the noncompensated aberration terms, such as vertical coma (Z7), which are included in total RMS.

The compensation of corneal astigmatism by internal astigmatism is well known (Le Grand & El Hage, 1980; Southall, 1937), and so our result of compensation for corneal horizontal/vertical astigmatism (Z5, 41% reduction) by the internal optics is not surprising. Artal et al. (2001) found the same compensation in term Z5. They also found compensation in triangular astigmatism (or trefoil, Z6), whereas we did not. Our ocular Z6 coefficient is, in fact, larger than the corneal coefficient. This discrepancy may be due to the difference in sample sizes (6 vs. 30 subjects).

The comparison of internal and corneal horizontal/vertical (H/V) astigmatism coefficients for each eye showed a significant negative correlation, indicating that the magnitude of the reduction in the H/V astigmatism of the complete eye is not randomly determined. If overall compensation were due simply to the pairing of a cornea and lens with coefficients inherently opposite in sign, then a mix of over- and under-compensation would be expected. Our data show a consistent match between the magnitudes of the corneal and internal coefficients, which suggests that a process exists to fine-tune H/V astigmatism compensation for the eye, at least in its relaxed accommodative state. Because the matching is so individual-specific, it is imaginable that this fine-tuning process is feedback driven and developmental. It is well documented that the prevalence of refractive astigmatism decreases from infancy to adulthood (Benjamin, 1998; Howland, Atkinson, Braddick, & French, 1978). Perhaps this ontogenetic decrease is due to the progressive development of compensation.

It is interesting to note that while H/V corneal astigmatism (Z5) was significantly compensated, corneal oblique astigmatism, Z3, was not. This may be due to the fact that only 3 of 30 subjects had oblique cylindrical meridians. It is possible that in a larger population of subjects with oblique astigmatism, compensation will be found.

In contrast to H/V astigmatism, spherical aberration does not show individual compensation, but scattered over-

and under-compensation regardless of corneal coefficient magnitude (Figure 7). Our interpretation of this result is that the compensation observed across the sample population is a reflection of the opposite signs of the spherical aberration inherent in the shapes and refractive properties of the cornea and lens. This compensation has been determined over the course of evolution by the feedback-process of natural selection. In one individual lifetime, compensation of spherical aberration is genetically programmed and occurs passively.

Lateral coma shows strong individual compensation. However, the magnitudes of corneal and internal lateral coma are also significantly correlated with the degree of noncoincidence of the Purkinje image and the center of the pupil (which indicates a nonzero angle kappa and/or an eccentricity of the pupil, Figure 9). The ray-tracing simulations through both the Navarro et al. and the Liou and Brennan schematic eye models (Figure 10) demonstrate that angle kappa itself may be responsible for some of the compensation of corneal lateral coma by internal coma that we observed in our measurements. Displacement of the pupil, the other cause of noncoincidence of the Purkinje image and the pupil center, does not cause automatic coma compensation in the Navarro schematic eye, but does in the Liou and Brennan eye (Figure 11). Despite the differences in ray-tracing outcomes for the two models, what is apparent is that shifting the location and alignment of the optical elements of the eye may be a very valid and simple mechanism by which compensation is generated. The individually scaled compensation seen in our lateral coma regression plot (Figure 6) suggests a process to minimize lateral coma in the eye at relaxed accommodation, which, such as that for astigmatism, could be developmental in nature. Subtle positioning of the optical elements may be a mechanism by which it is achieved.

Relative to increasing ocular total high-order wavefront error, the reduction in RMS error introduced by lateral coma plus spherical aberration compensation (Z8+Z12) seems to be gradually countered by the error introduced by uncompensated aberrations. As seen in Figure 8a, the RMS magnitude of Z8+Z12 compensation stays within an approximate range for increasing levels of high-order ocular aberration. However, total high-order compensation, the difference in magnitude between ocular and corneal coefficients, decreases with increasing ocular total aberration (Figure 8b). In more highly aberrated eyes, the uncompensated terms counteract the compensation generated by Z8 and Z12, to the point where total ocular wavefront error is actually greater than corneal wavefront error. The uncompensated RMS error must be primarily generated by the internal optics, because corneal wavefront error does not significantly change as ocular wavefront error increases (Figure 8c). Thus, that Z8+Z12 compensation occurs does not ensure an eye with low wavefront aberration. However, as lateral coma and spherical aberration are the two high-order terms that are largest in magnitude (Figure 3), their compensation nonetheless has a role in keeping ocular aberration levels low.

In all of our comparisons, we have said that the internal optics compensate for the cornea, rather than vice versa. This is because as the eye ages, it is primarily the changes in the lens that cause the disappearance of compensation and the augmentation of ocular aberrations (Artal et al., 2002). The lens continuously grows, and over the course of life, its spherical aberration coefficient reverses sign and increases in magnitude (Glasser & Campbell, 1998). Internal optics aberrations increase three-fold between ages 20 and 70 years, whereas corneal aberrations increase only mildly (Artal et al., 2002). The decreasing diameter of the pupil with age limits the influence that changes in corneal aberration structure have on image optical quality. Oshika, Klyce, Applegate, and Howland (1999) found that in a 7-mm pupil, corneal aberrations increased significantly with age, but that for a 3-mm pupil, there was no significant increase.

Our data concerning astigmatism and lateral coma suggest a process to fine-tune the compensation between the cornea and internal optics. In exploring this possibility, we should not make the assumption that the internal optics are determined as a match for the corneal surface. Both elements are capable of changing over time, and we do not know if aberrations in one drive the other or if it is a mutual optimization process.

The time course and mechanism of such an "emmetropization" process are still to be determined. Perhaps a reshuffling of the gradient refractive index of the lens is involved. Previous studies have suggested this as a mechanism for the lens's maintenance of the same focal length despite changes in surface curvature that occur with age (Glasser & Campbell, 1998; Smith, Atchison, & Pierscionek, 1992). Artal et al. (2001) suggested that subtle tilting and decentering of the lens to produce lower order aberrations might be a simple way to balance the cornea and internal optics, and we have already mentioned this as a solution specific to lateral coma. Another possibility is that the posterior surface of the cornea has a substantial compensatory role but has not yet been measured (Artal et al., 2001). Also, the persistence or disappearance of compensation with accommodation has not been addressed here. Future studies on the accommodative and ontogenetic changes in aberration structure should provide further insights.

Acknowledgments

We thank the National Institutes of Health for grant NIH NEI EY-02994 to HCH.

Commercial relationships: none.
Corresponding author: Jennifer Kelly.
Email: jek25@cornell.edu.
Address:W203 Mudd Hall, Department of Neurobiology and Behavior, Cornell University, Ithaca, NY, 14853.

References

Artal, P., & Guirao, A. (1998). Contributions of the cornea and lens to the aberrations of the human eye. *Optics Letters, 23,* 1713-1715.

Artal, P., Guirao, A., Berrio, E., & Williams, D. R. (2001). Compensation of corneal aberrations by the internal optics of the human eye. *Journal of Vision, 1,*(1) 1-8, http://journalofvision.org/1/1/1/, doi:10.1167/1.1.1. [PubMed] [Article]

Artal, P., Berrio, E., Guirao, A., & Piers, P. (2002). Contribution of the cornea and internal surfaces to the change of ocular aberrations with age. *Journal of the Optical Society of America A, 19,* 137-143. [Pubmed]

Benjamin, W. J. (Ed.)(1998). *Borish's clinical refraction.* Philadelphia: W. B. Saunders Company.

El Hage, S., & Berny, F. (1973). Contribution of the crystalline lens to the spherical aberration of the eye. *Journal of the Optical Society of America, 63,* 205-211. [Pubmed]

Glasser, A., & Campbell, M. C. W. (1998). Presbyopia and the optical changes in the human crystalline lens with age. *Vision Research, 38,* 209-229. [Pubmed]

Guirao, A., & Artal, P. (2000). Corneal wave aberration from videokeratography: Accuracy and limitations of the procedure. *Journal of the Optical Society of America A, 17,* 955-965. [Pubmed]

Howland, H. C., Glasser, A., & Applegate, R. (1992). Polynomial approximations of corneal surfaces and corneal curvature topography. *OSA 1992 Technical Digest Series on Ophthalmic and Visual Optics, 3,* 34-37.

Howland, B., & Howland, H. C. (1977). A subjective method for the measurement of monochromatic aberrations of the eye. *Journal of the Optical Society of America, 67,* 1508-1517. [Pubmed]

Howland, H. C., Atkinson, J., Braddick, O., & French, J. (1978). Infant astigmatism measured by photorefraction. *Science, 202,* 331-333. [Pubmed]

Jahns, J., & Walker, S. J. (1990). Two-dimensional array of diffractive microlenses fabricated by thin film deposition. *Applied Optics, 7,* 931-936.

Le Grand, Y., & El Hage, S. G. (1980). *Physiological optics* (pp. 153). New York: Springer-Verlag.

Liou, H. L., & Brennan, N. A. (1997). Anatomically accurate, finite model eye for optical modeling. *Journal of the Optical Society of America A, 14,* 1684-1695. [Pubmed]

Navarro, R., Santamaria, J., & Bescos, J. (1985). Accommodation-dependent model of the human eye with aspherics. *Journal of the Optical Society of America A, 2,* 1273-1281. [Pubmed]

Oshika, T., Klyce, S. D., Applegate, R. A., & Howland, H. C. (1999). Changes in corneal wavefront aberrations with aging. *Investigative Ophthalmology & Visual Science, 40,* 1351-1355. [Pubmed]

Rand, R. H., Howland, H. C., & Applegate, R. A. (1997). Mathematical model of a placido disk keratometer and its implications for recovery of corneal topography. *Optometry and Vision Science, 74,* 926-930. [Pubmed]

Salmon, T. O., & Thibos, L. N. (2002). Videokeratoscope-line-of-sight misalignment and its effect on measurements of corneal and internal ocular aberrations. *Journal of the Optical Society of America A, 19,* 657-669. [Pubmed]

Schwiegerling, J., Greivenkamp, J. E., & Miller, J. M. (1995). Representation of videokeratoscopic height data with Zernike polynomials. *Journal of the Optical Society of America A, 12,* 2105-2113. [Pubmed]

Smith, G., Atchison, D. A., & Pierscionek, B. K. (1992). Modeling the power of the aging human eye. *Journal of the Optical Society of America A, 9,* 2111-2117. [Pubmed]

Smith, G., Cox, M. J., Calver, R., & Garner, L. F. (2001). The spherical aberration of the crystalline lens of the human eye. *Vision Research, 41,* 235-243. [Pubmed]

Smith, G. (1995). Schematic eyes: History, description and applications. *Clinical and Experimental Optometry, 78,* 176-189.

Smolek, M. K., Klyce, S. D., & Sarver, E. J. (2002). Inattention to nonsuperimposable midline symmetry causes wavefront analysis error. *Archives of Ophthalmology, 120,* 439-447. [Pubmed]

Southall, J. P. C. (1937). *Introduction to physiological optics* (pp. 54-59, 148-149). New York: Oxford University Press.

Thibos, L. N., & Hong, X. (1999). Clinical applications of the Shack-Hartmann aberrometer. *Optometry and Visual Science, 76,* 817-825. [Pubmed]

van Meeteren, A., & Dunnewold, C. J. (1983). Image quality of the human eye for eccentric entrance pupils. *Vision Research, 23,* 573-579. [Pubmed]